Biochemistry

 Volume 36, Number 45 November 11, 1997

New Concepts in Biochemistry

Single Binding Versus Single Channel Recordings: A New Approach to Study Ionotropic Receptors†

Stuart J. Edelstein,*,‡,§ Olivier Schaad,‡ and Jean-Pierre Changeux§

Département de Biochimie, Université de Genève, CH-1211 Genève 4, Switzerland and Neurobiologie Moléculaire, Institut Pasteur, 75734 Paris Cedex 15, France

Received July 28, 1997; Revised Manuscript Received September 23, 1997⊗

ABSTRACT: The observation of ligand binding to a single molecule has become feasible with recent developments in laser-based fluorescence microscopy. We have simulated such single ligand-binding events for the nicotinic acetylcholine receptor in order to provide comparisons with single channel events under pulsed agonist conditions. The binding events would be more complex than ionic events due to multiple interconversions between different conformational states at the same degree of ligation. Nevertheless, recording of such events could provide valuable new information concerning the role of ligand binding in stabilizing conformational changes and the degree of functional nonequivalence of the binding sites.

Ligand-gated channels mediate rapid chemical signaling at synapses. Upon quantal release from the presynaptic surface, neurotransmitters bind to receptors on the postsynaptic membrane with rates near the diffusion limit; the binding shifts the receptor to the open-channel state, initiating a transient ion flux terminated by return to the basal (resting) state, or by transition to a desensitized state. Many of these principles were derived from experimental and theoretical studies on the nAChR[1] from fish electric organ or the neuromuscular junction (*1*−*8*). The muscle nAChR is a heteropentameric [2α:1β:1γ/ϵ:1δ] integral membrane protein (*6*) with an axial ion channel bordered by the M2 transmembrane segment (*9*−*11*) and with the subunit order α-γ-α-δ-β (*12*), although alternative interpretations have been proposed (*13*). Accumulating evidence (*14*−*19*) suggests that for each ACh site a "principal component" is contributed by the α subunits and a "complementary" component (*20*) by the adjacent γ or δ subunit. The two structurally distinct sites may lead to functional differences. Stronger binding has been attributed to the site at the α/δ interface for agonists (*21*−*23*) but to the site at the α/γ interface for the competitive antagonist *d*-tubocurarine (*15*). Moreover, the site of stronger binding may depend on the conformational state, as could be determined with receptors fixed in a particular state (*24*).

† The research reported here was supported by the Swiss National Science Foundation, the Société Académique de Genève, the Association Française Contre Les Myopathies, the Collège de France, the Centre National de la Recherche Scientifique, the Institut National de la Santé et de la Recherche Médicale, the Direction des Recherches Etudes et Techniques, Human Frontiers, EEC Biotech and Biomed, and the Council for Tobacco Research.

* To whom correspondence should be addressed. Department of Biochemistry, 30 quai Ernest-Ansermet, CH-1211 Genève 4, Switzerland. E-mail: Stuart.Edelstein@biochem.unige.ch. Telephone: (41−22) 702−6486. Fax: (41−22) 702−6476.

‡ Université de Genève.

§ Institut Pasteur.

⊗ Abstract published in *Advance ACS Abstracts,* October 15, 1997.

[1] Abbreviations: nAChR, nicotinic acetylcholine receptor; ACh, acetylcholine; pdf, probability density function; EC_{50}, equilibrium concentration at 50% response.

S0006-2960(97)01830-8 CCC: $14.00

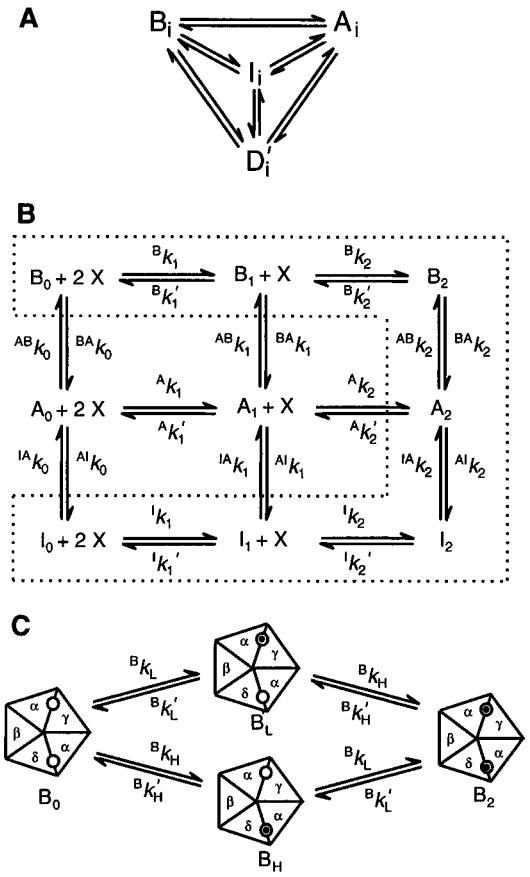

FIGURE 1: Conformational states and ligand-binding reactions for nAChR with two agonist sites. (A) All interconversion reactions for receptors in the B, A, I, and D states. (B) The allosteric-type model with B, A, and I states. The equilibrium constants may be defined from the kinetic constants for ligand reactions (i.e., ${}^{B}K = {}^{B}k'_1/{}^{B}k_1$) or isomerization (i.e., ${}^{BA}L_0 = {}^{AB}K_0/{}^{BA}K_0$). The sequential-type model is limited to the reactions within the dashed enclosure, with formation of the open state (A_2) from B_2 defined by $K_{open} = [B_2]/[A_2] = \alpha/\beta$, where $\alpha = {}^{AB}k_2$ and $\beta = {}^{BA}k_2$. In some cases, the sequential model has been extended to the singly liganded open state (A_1) to account for brief openings (*26*). (C) Subunit structure and ligand binding sites at the α/γ and α/δ interfaces within the B state. Ligand occupancy at the higher and lower affinity sites are designated by the subscripts H and L, respectively, with ${}^{B}K_H = {}^{B}k'_H/{}^{B}k_H$, ${}^{B}K_L = {}^{B}k'_L/{}^{B}k_L$ (if ${}^{B}K_H \ll {}^{B}K_L$, $K_1 = {}^{B}K_H$ and $K_2 = {}^{B}K_L$, but the exact values are $K_1 = {}^{B}K_H{}^{B}K_L/[{}^{B}K_H + {}^{B}K_L]$ and $K_2 = {}^{B}K_H + {}^{B}K_L$). For identical sites, where ${}^{B}K = {}^{B}K_H = {}^{B}K_L$, the values of K_1 and K_2 are set by $K_1 = {}^{B}K/2$ and $K_2 = 2{}^{B}K$. These distinctions for H and L affinity sites may be applied to the A and I states.

Single channel measurements on muscle nAChR have contributed to the understanding of these receptors by providing high temporal resolution and access to the properties of individual molecules (*25*, *26*). However, the linked events of ligand binding have only been inferred *indirectly*, since parallel observations on binding steps have not been possible. While a single channel event triggers the flux of thousands of ions, no such amplification is produced by a single binding event. Yet, developments in the field of laser-based fluorescence microscopy (*27*−*32*) now place such measurements in the realm of possibilities in conjunction with suitable fluorescent agonists (*33*, *34*). This approach relies on a narrow laser beam (radius ≈ 0.2 μM) that illuminates such small volumes that only one or several molecules are excited. Therefore, we have undertaken simulations in order to study what additional insights would be available from measurements that follow simultaneously both single ionic and binding events. In this respect, theory precedes experiment, but should provide a stimulus for the necessary experimental advances.

Table 1: Rates for Ligand Binding and Conformational Transitions of nAChR[a]

		equivalent sites	H site	L site
ligand on-rates	${}^{B}k$	1.5	1.0	0.05
($\times 10^8$ M^{-1} s^{-1})	${}^{A}k$	1.5	1.0	1.0
	${}^{I}k$	1.5	1.0	1.0
ligand off-rates (s^{-1})	${}^{B}k'$	8000	500	1.8×10^4
	${}^{A}k'$	8.6	2.5	30
	${}^{I}k'$	4.0	4.0	
transition rates (s^{-1})	${}^{BA}k_0$	0.534	0.028	
	${}^{BA}k_1$	126.5	1.8	44
	${}^{BA}k_2$	30 000	2800	
	${}^{AB}k_0$	1.078×10^4	5013	
	${}^{AB}k_1$	2747	1604	670
	${}^{AB}k_2$	700	214	
	${}^{AI}k_0$	19.85	19.7	
	${}^{AI}k_1$	19.93	19.85	
	${}^{AI}k_2$	20	20	
	${}^{IA}k_0$	1.65	3.78	
	${}^{IA}k_1$	1.16	1.73	
	${}^{IA}k_2$	0.81	0.81	

[a] The parameters corresponding to the equivalent site data are based on published values derived from single channel measurements (*26*) and rapid agonist application (*48*), with the full set of interconversion rates calculated using linear free-energy relations (*8*). Parameters for nonequivalent sites were derived from the data of Jackson (*45*), with corrections (*49*) incorporated, and small adjustments made to permit agreement with the linear transition state theory and the binding scheme presented in Figure 1C. Since no information on the nonequivalence of sites for the I or D states has been reported (*45*), identical sites were assumed.

Theoretical Considerations. Single channel stochastic simulations are relatively straightforward (*35*), since channels generally alternate between discrete open and closed states.[2] In contrast, single binding events may be complicated by possible multiple passages through different conformational states at the same degree of ligation. Therefore, a theory that distinguishes between single binding and single ionic events has been formulated, based on the central assumption of the allosteric model that postulates distinct "state" and "binding" functions (*36*−*38*). The model is further assumed to include multiple conformational states (*8*) and two potentially nonequivalent sites. Chemical kinetics *in vitro* (*33*, *39*) and single channel recordings (*25*) are consistent with interconversions of the receptor molecule between at least four conformational states: a closed but activatable B (basal) state, an open channel A (active) state, an initial desensitized I state, and a deeply desensitized D state.

With four interconverting conformational states, the transition reactions can be described by a tetrahedral scheme (Figure 1A). However, since reaction rates between interconverting pairs of states differ widely for nAChR, the predominant kinetic pathway leads to a linear scheme B $\rightleftarrows$ A $\rightleftarrows$ I $\rightleftarrows$ D that provides a satisfactory description of experimental data with the simplification resulting in errors

[2] More complex patterns can occur, however, as for certain high-affinity channel mutants such as ϵT264P (*50*). In this case, the data suggest an intrinsic B $\rightleftarrows$ A equilibrium less strongly in favor of B than for wild-type receptors, i.e., the mutant exhibits an L phenotype (*51*), resulting in a decrease of the $A_2 \rightarrow B_2$ rate into the range of the A_2 off-rate, such that a significant fraction of the A_2 open channel events are predicted to terminate by passage to A_1 (*52*).

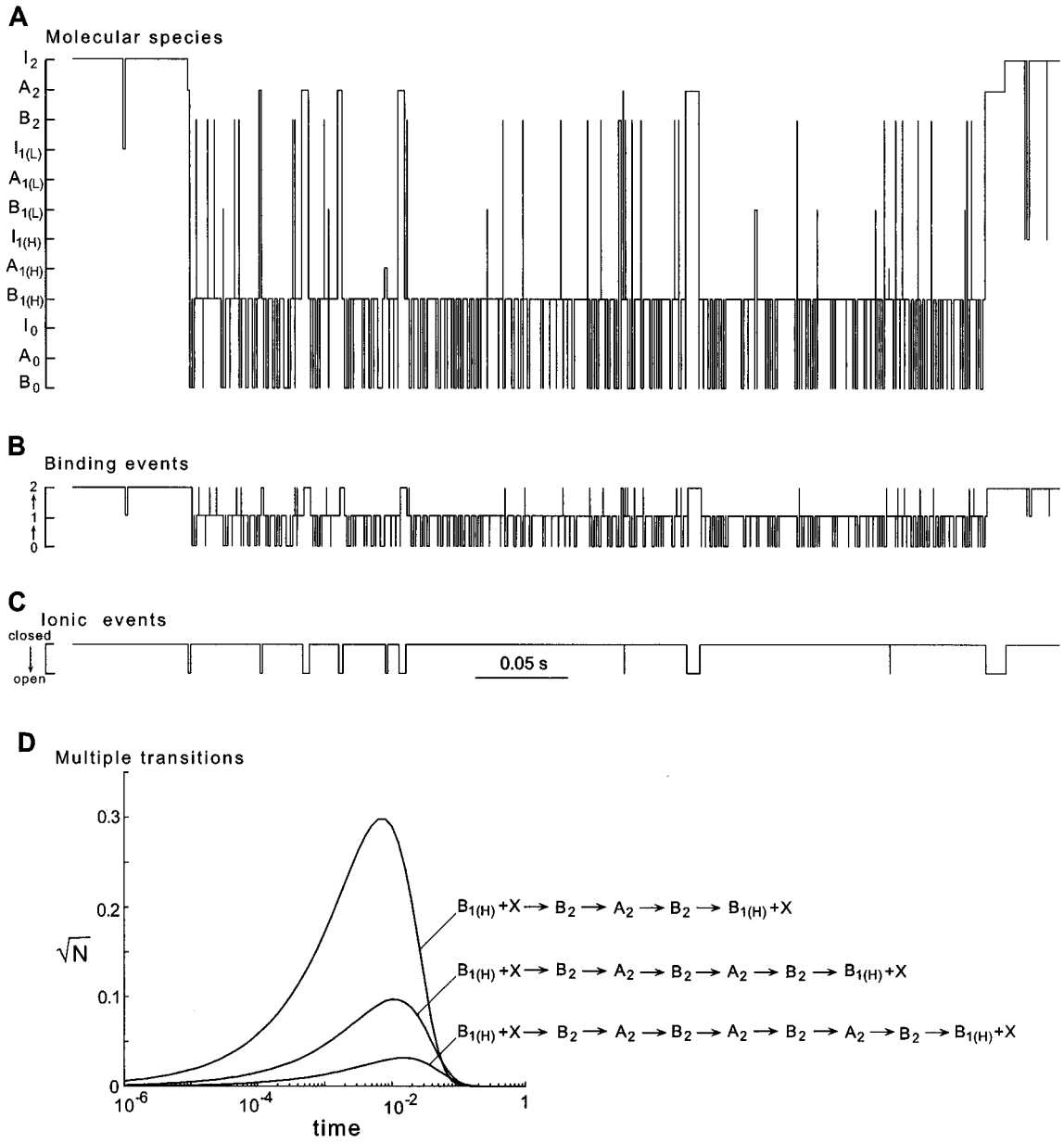

FIGURE 2: Stochastic simulations of ligand binding and conformational transitions for a receptor with two nonequivalent sites. (A) Passages among all possible molecular species (except D state). (B) Passages scored as binding events. (C) Passages scored as ionic events. (D) Multiple transitions between conformational states. The simulations were conducted with the previously described program (*8*) applied to nonequivalent ligand-binding sites using the parameters in Table 1. All calculations were based on a ligand concentration of 2×10^{-5} M. For the species with one molecule of agonist bound, its presence on the high or low affinity site is noted, respectively, by H or L in the subscript, e.g., $B_{1(H)}$ or $B_{1(L)}$ for the B state. In panel D, the individual dwell time profiles are presented for B_2 binding events prolonged by passages to A_2. Each pdf is presented as the square root of the number of events versus time on a logarithmic scale and is defined by $g(x) = \sum_{j=1}^{m} a_j\, g_0\,(z_j)$, where a_j is the fractional amplitude of the jth component and $g_0\,(z_j) = \exp\,[z_j - \exp\,(z_j)]$, with $z_j = x - s_j$, $x = \ln t$, $t =$ time in seconds, and $s_j =$ logarithm of the jth time constant (*43*). Since the number of events is proportional to t (the length of time examined), f_j (the fractional concentration of the reacting component), and $1/\tau_j$ (the rate of the relevant reaction), the amplitude of the jth component is given by: $a_j = (f_j t)/\tau_j$. The peak height for a specific class of events is given by $N_j = (f_j t\, dx\, r_j[1 - p_j]e^{-1})/\tau_j$, where dx is the interval of ln t used to set the width of the bins, r_j is the relevant ratio of kinetic rates, $[1 - p_j]$ gives the fraction of events remaining after a series of passages to a neighboring state each with a probability of p_j, and e^{-1} corresponds to the maximum value of $g(x)$, which occurs at the logarithm of τ_j. For the simulations presented here d$x = 0.23$, corresponding to 10 bins for each integer interval of log t, with peak heights based on the number of events occurring in a total time t of 1 s. The term r_j is calculated from the appropriate rate constants of alternative pathways. For example, each passage via A_2 may be terminated by a transition (to I_2 or B_2) or by a ligand dissociation; hence, the probability of a transition to B_2 will be given (for nonequivalent binding sites) by $r_j = {}^{AB}k_2/({}^{AB}k_2 + {}^{A}k'_H + {}^{A}k'_L + {}^{AI}k_2)$. Successive passages correspond to the series of distinct pdf curves presented, with reduced probability and progressively longer characteristic values of the average τ_j. The probability for each successive passage to A_2 is diminished a factor, $p_j = [{}^{BA}k_2/({}^{BA}k_2 + {}^{B}k'_H + {}^{B}k'_L)][{}^{AB}k_2/({}^{AB}k_2 + {}^{A}k'_H + {}^{A}k'_L + {}^{AI}k_2)]$. The sum of all such events is given by the series $\sum S = 1 + p_j + p_j^2 + \ldots = 1/[1 - p_j]$ and the fraction of primary ligand-binding events without passage to another state is given by $[1 - p_j]$. The contributions of all prolongations are summed, added to the primary A state binding events, and the totals are indicated by $\sum A$ in Figure 3.

of <1% (*8*). At equilibrium, for moderate agonist concentrations, receptors would be mainly in the D state and single-binding and single-channel events would be infrequent. Therefore, for the examples analyzed here, it was assumed that application of agonist would occur as a pulse with a duration in the time range of seconds, such that the system

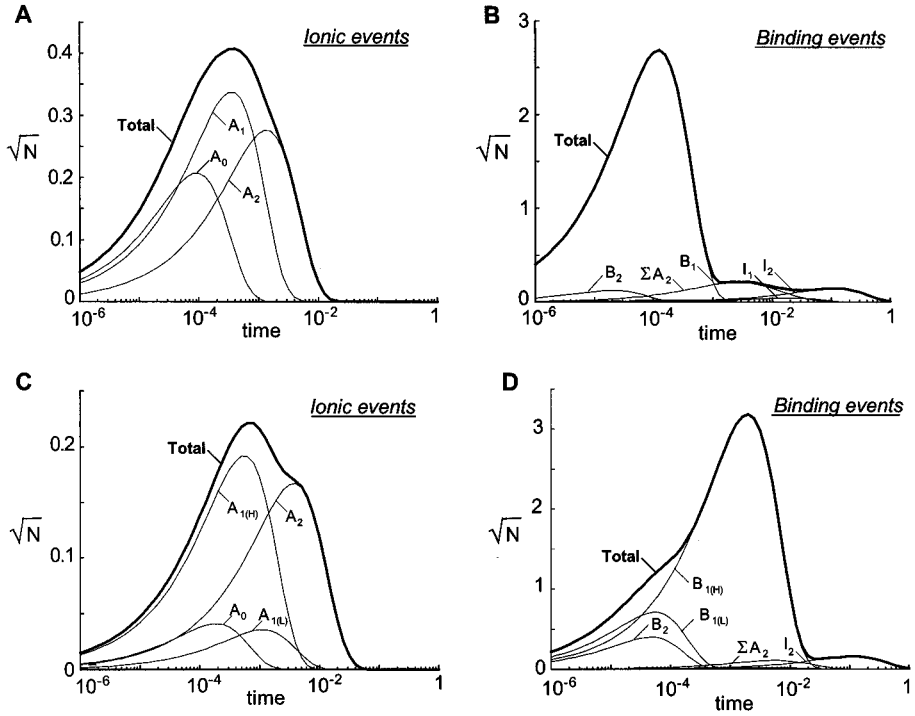

FIGURE 3: Dwell time probability profiles for stochastic simulations of binding events and ionic events for nAChR at low ligand concentrations. (A) Ionic events and (B) binding events for simulations based on data interpreted with equivalent sites. (C) Ionic events and (D) binding events for simulations based on data interpreted with nonequivalent sites. The dwell times are presented as the total events, corresponding to simulated experimental measurements (thick lines), along with the underlying contributions of the individual components (thin lines). The simulations are based on the values in Table 1 and a ligand concentration of $X = 0.3\ \mu$M in panels A and B and $X = 1.7\ \mu$M in panels C and D, corresponding in both cases to a probability of channel opening, $P_{open} = 0.002$ computed with the equation $P_{open} = 1/(1 + K_{open}[({}^{B}K_1{}^{B}K_2)/[X]^2 + {}^{B}K_2/[X] + 1]/[({}^{A}K_1{}^{A}K_2)/[X]^2 + {}^{A}K_2/[X] + 1])$, where the equilibrium constants are defined in Figure 1. Other details as described in Figure 2.

could only progress to the first (I) desensitized state (Figure 1B). This representation may be contrasted with the standard sequential model (*26*) based on the different assumption of a conformational change induced by and concurrent with ligand binding, as proposed for soluble enzymes (*40*, *41*) and observed, for example, in the substrate-induced changes in carboxypeptidase A in the region of Tyr-248 (*42*). Formally, the binding and conformational events of the sequential scheme would be limited to the steps within the dashed enclosure of Figure 1B. Each of the conformational states may be characterized by a potentially distinct affinity for ligand at each of the two binding sites (Figure 1C).

When the allosteric model is evaluated in stochastic simulations, trains of molecular forms are generated that vary with respect to the conformational state and/or the degree of binding site occupancy (Figure 2A). Each change in the number of ligands bound is scored as a binding event (Figure 2B) and each transition to an A-state molecular species is scored as an ionic event (Figure 2C). Hence, Figure 2, panels B and C, correspond to measurements that are expected to be produced experimentally in joint single binding and single channel recordings. These stochastic simulations extending over 0.5 s only partially illustrate the behavior of the system. A more complete description is provided by the probabilities of events for each time interval (bin width) sampled, leading to the "probability density function" or "pdf" (*35*, *43*). However, since ligand-binding dwell times will be lengthened by multiple passages between two conformational states at the same degree of ligand saturation, the contributions to the total binding events of all such multiple passages (which for nAChR involve the A state) must be included, as illustrated in Figure 2D. This analysis permits the complexity of binding events to be anticipated and potentially to provide information on the mechanism of signal transduction that would not be available from single channel recordings alone. For example, it would be possible to resolve the contributions of the two potentially nonequivalent binding sites, as illustrated in the following section.

Simulations Comparing Equivalent and Nonequivalent Sites. For muscle nAChR, two equivalent sites were used to model single channel measurements (*7*, *26*, *44*). Yet, in a number of other studies the data were interpreted on the basis of marked differences (up to 700-fold; see Table 1) in the affinities of the two ligand-binding sites (*45*−*47*). Species differences and dependence on expression systems may be responsible in part for the lack of agreement on the characteristics of the two binding sites (*7*), but uncertainties remain concerning their intrinsic functional properties. Therefore, simulations were conducted to determine whether measurements of single binding events in conjunction with single ionic events could resolve the extent of nonequivalence of the binding sites and reveal differences in the predictions of the allosteric and sequential models.

For simulated recordings of muscle AChR at low ligand concentrations, only minor differences are predicted for dwell time profiles of ionic events with parameters based on analyses with equivalent (Figure 3A) versus nonequivalent sites (Figure 3C). At the concentrations of these simulations, ionic events are predicted to be rare, ~1/s (corresponding to a probability of channel opening of $P_{open} = 0.002$), whereas binding events are predicted to be at least an order of magnitude more abundant (Figure 3 panels B and D). With respect to the two principal models, for both equivalent (Figure 3A) and nonequivalent sites (Figure 3C), more ionic

events (at shorter average times) are predicted by the allosteric model (thick lines) compared to the sequential model (thin lines corresponding to the A_2, the only molecular species producing ionic events in the sequential model).

With the parameters based on nonequivalent sites, the shoulder at longer times ($\sim 10^{-2}$ s) on the profile of ionic events in Figure 3C is slightly more pronounced, and at all concentrations, fewer events are predicted than for equivalent sites, due to a lower estimate for the value of $^{AB}k_2$ (Table 1). However, for single channel experimental data with the usual limits of precision, it would be difficult to distinguish between the equivalent and nonequivalent interpretations. It can thus be concluded that a compensation of parameters leads to similar properties in the two cases. This compensation may explain why experimental single channel recordings have been interpreted with equivalent sites in some cases and with nonequivalent sites in other cases (*7*). As a result, meaningful conclusions cannot readily be drawn from single ion channel recordings alone.

In contrast to the similarity of ionic events, larger differences in the simulated binding events are predicted for equivalent sites (Figure 3B) versus nonequivalent sites (Figure 3D). In the latter case, binding of the first ligand to a receptor molecule is predicted to occur almost exclusively at the higher affinity site to generate $B_{1(H)}$. Since an off-rate 16-fold lower than in the case of equivalent sites was deduced (Table 1), the peak in the dwell time profile for binding events is predicted to lie at significantly longer times: 2×10^{-3} s for nonequivalent sites (Figure 3D) compared to 1.2×10^{-4} s for equivalent sites (Figure 3B). Hence, if single ligand-binding events were measured experimentally, their dwell time profiles could provide a direct test of the extent of binding site nonequivalence.

At higher ligand concentrations corresponding to a probability of channel opening of $P_{open} = 0.5$ (data not shown), the simulated ionic events arise mainly from transitions to A_2 and are anticipated to be almost as abundant as the binding events. As a consequence, the predictions of the allosteric and sequential models are virtually identical for ionic events, and very similar binding events are also predicted for both equivalent and nonequivalent sites. Therefore, experiments at low ligand concentrations should be favored in order to distinguish between allosteric versus sequential models and equivalent versus nonequivalent sites.

Concluding Remarks. The concept of single ligand binding versus single channel recordings presented here could provide new insights into the mechanism of ligand-gated channels. In particular, such measurements could be utilized to evaluate more critically the degree of nonequivalence of the ligand-binding sites. With respect to the allosteric-type and the more restricted sequential-type functional models, the simulations demonstrate that for wild-type receptors significant differences are predicted for single channel measurements, but only at low ligand concentrations (Figure 3). Under these conditions, the allosteric model predicts appreciable contributions to channel opening from nonliganded and monoliganded receptors, in contrast to the sequential model which limits channel opening only to biliganded receptors (A_2). As a result, compared to the allosteric model, the sequential model predicts fewer ionic events and events with an average dwell time about 4 times longer. Therefore, the quantitative differences between the frequencies and durations of opening events predicted by the two models represent a testable criterion to distinguish between models in suitably designed experiments.

A number of other issues remain to be clarified concerning the fundamental properties of ligand-gated channels. Information on their three-dimensional structure at atomic resolution would provide a necessary context for developing mechanistic models at the molecular level. In addition, dynamic approaches will be required to elucidate the role of the conformational changes associated with agonist binding and may involve the development of novel methods. In this context, "single binding" versus "single channel" recordings offer new parameters that should facilitate progress in the domain of structure-function relations in the course of signal transduction and its short time regulation.

REFERENCES

1. Devillers-Thiéry, A., Galzi, J.-L., Eiselé, J.-L., Bertrand, S., Bertrand, D., and Changeux, J.-P. (1993) *J. Membr. Biol. 136*, 97−112.
2. Hess, G. P. (1993) *Biochemistry 32*, 989−1000.
3. Unwin, N. (1993) *Neuron 10*, 31−41.
4. Bertrand, D., and Changeux, J.-P. (1995) *Semin. Neurosci. 7*, 75−90.
5. Galzi, J.-L., and Changeux, J.-P. (1995) *Neuropharmacology 34*, 563−582.
6. Karlin, A. and Akabas, M. H. (1995) *Neuron 15*, 1231−1244.
7. Edmonds, B., Gibb, A. J., and Colquhoun, D. (1995) *Annu. Rev. Physiol. 57*, 469−493.
8. Edelstein, S. J., Schaad, O., Henry, E., Bertrand, D., and Changeux, J.-P. (1996) *Biol. Cybern. 75* , 361−380.
9. Giraudat, J., Dennis, M., Heidmann, T., Chang, J. Y., and Changeux, J.-P. (1986) *Proc. Natl. Acad. Sci. U.S.A. 83*, 2719−2723.
10. Hucho, F., Oberthur, W., and Lottspeich, F. (1986) *FEBS Lett. 205*, 137−142.
11. Imoto, K., Busch, C., Sakmann, B., Mishina, M., Konno, T., Nakai, J., Bujo, H., Mori, Y., Fukuda, K., and Numa, S. (1988) *Nature 335*, 645−648.
12. Machold, J., Weise, C., Utkin, Y., Tsetlin, V., and Hucho, F. (1995) *Eur. J. Biochem. 234*, 427−430.
13. Unwin, N. (1996) *J. Mol. Biol. 257*, 586−596.
14. Oswald, R. E., and Changeux, J.-P. (1982) *FEBS Lett. 139*, 225−229.
15. Pedersen, S. E., and Cohen, J. B. (1990) *Proc. Natl. Acad. Sci. U.S.A. 87*, 2785−2789.
16. Chatrenet, B., Trémeau, O., Bontems, F., Goeldner, M. P., Hirth, C. G., and Ménez, A. (1990) *Proc. Natl. Acad. Sci. U.S.A. 87*, 3378−3382.
17. Galzi, J.-L., Revah, F., Bouet, F., Ménez, A., Goeldner, M., Hirth, C., and Changeux, J.-P. (1991) *Proc. Natl. Acad. Sci. U.S.A. 88*, 5051−5055.
18. Czajkowski, C., Kaufmann, C., and Karlin, A. (1993) *Proc. Natl. Acad. Sci. U.S.A. 90*, 6285−6289.
19. Fu, D. X., and Sine, S. M. (1994) *J. Biol. Chem. 269*, 26152−26157.
20. Corringer, P. J., Galzi, J.-L., Eiselé, J.-L., Bertrand, S., Changeux, J.-P., and Bertrand, D. (1995) *J. Biol. Chem. 270*, 11749−11752.
21. Blount, P., and Merlie, J. P. (1989) *Neuron 3*, 349−357.
22. Sine, S. M., and Claudio, T. (1991) *J. Biol. Chem. 266*, 19369−19377.
23. Prince, R. J., and Sine, S. M. (1996) *J. Biol. Chem. 271*, 25770−25777.
24. Watty, A., Methfessel, C., and Hucho, F. (1997) *Proc. Natl. Acad. Sci. U.S.A. 94*, 8202−8207.
25. Sakmann, B., Patlak, J., and Neher, E. (1980) *Nature 286*, 71−73.
26. Colquhoun, D., and Sakmann, B. (1985) *J. Physiol. 369*, 501−557.
27. Eigen, M., and Rigler, R. (1994) *Proc. Natl. Acad. Sci. U.S.A. 91*, 5740−5747.

28. Mertz, J., Wu, C., and Webb, W. W. (1995) *Optics Lett. 20*, 2532−2534.
29. Edman, L., Mets, U., and Rigler, R. (1996) *Proc. Natl. Acad. Sci. U.S.A. 93*, 6710−6715.
30. Rauer, B., Neumann, E., Widengren, J., and Rigler, R. (1996) *Biophys. Chem. 58*, 3−12.
31. Xie, X. S. (1996) *Acc. Chem. Res. 29*, 598−606.
32. Schwille, P., Meyer-Almes, F.-J., and Rigler, R. (1997) *Biophys. J. 72*, 1878−1886.
33. Heidmann, T., and Changeux, J.-P. (1980) *Biochem. Biophys. Res. Commun. 97*, 889−896.
34. Valenzuela, C. F., Weign, P., Yguerabide, J., and Johnson, D. A. (1994) *Biophys. J. 66*, 674−682.
35. Colquhoun, D., and Hawkes, A. G. (1995) in *Single-Channel Recording* (Sakmann, B., & Neher, E., Eds.) pp 397−482, Plenum Press, New York.
36. Monod, J., Wyman, J., and Changeux, J.-P. (1965) *J. Mol. Biol. 12*, 88−118.
37. Rubin, M. M., and Changeux, J.-P. (1966) *J. Mol. Biol. 21*, 265−274.
38. Edelstein, S. J., and Changeux, J.-P. (1996) *Experientia 52*, 1083−1090.
39. Neubig, R. R., and Cohen, J. B. (1980) *Biochemistry 19*, 2770−2779.
40. Koshland, D. E. (1963) *Cold Spring Harbor Symp. Quant. Biol. 28*, 473−480.
41. Koshland, D. E., Némethy, G., and Filmer, D. (1966) *Biochemistry 5*, 365−385.
42. Christianson, D. W., and Lipscomb, W. N. (1989) *Acc. Chem. Res. 22*, 62−69.
43. Sigworth, F. J., and Sine, S. M. (1987) *Biophys. J. 52*, 1047−1054.
44. Lingle, C. J., Maconochie, D., and Steinbach, J. H. (1992) *J. Membr. Biol. 126*, 195−217.
45. Jackson, M. B. (1988) *J. Physiol. 397*, 555−583.
46. Sine, S. M., Claudio, T., and Sigworth, F. J. (1990) *J. Gen. Physiol. 96*, 395−437.
47. Zhang, Y., Chen, J., and Auerbach, A. (1995) *J. Physiol. 486*, 189−206.
48. Franke, C., Parnas, H., Hovav, G., and Dudel, J. (1993) *Biophys. J. 64*, 339−356.
49. Jackson, M. B. (1993) in *Thermodynamics of membrane receptors and channels* (Jackson, M. B., Ed.) pp 249−293, CRC Press, Boca Raton.
50. Ohno, K., Hutchison, D. O., Milone, M., Brengman, J. M., Bouzat, C., Sine, S. M., and Engel, A. G. (1995) *Proc. Natl. Acad. Sci. U.S.A. 92*, 758−762.
51. Galzi, J.-L., Edelstein, S. J., and Changeux, J.-P. (1996) *Proc. Natl. Acad. Sci. U.S.A. 93*, 1853−1858.
52. Edelstein, S. J., Schaad, O., and Changeux, J.-P. (1997) *CR Acad. Sci. Paris* (in press).

BI9718301